

Experimental study on inflatable circular diaphragms used in the oscillating water column wave energy converter

F. Abad*, S. Lotfian, S. Dai, G. Zhao, G. Alarcon, L. Yang, Y. Huang, Q. Xiao, F. Brennan
Faculty of Engineering, University of Strathclyde, Glasgow G4 0LZ, UK

*Corresponding author: Email: farhad.abad@strath.ac.uk

ABSTRACT: Wave Energy Converters (WECs) convert ocean waves' kinetic and potential energy into electricity. This paper studies the effect of different parameters on an Inflatable Circular Diaphragm (ICD) used in a WEC device. A small-scale Oscillating Water Column (OWC) with an elastomer part at the top of the air chamber is considered, and several experiments on the water tank and dry test rig are conducted. In the first part, the experimental results of an OWC with an ICD in the small water tank are presented, and the effect of wave height and frequency on the deformation of an elastomer is studied. In the second part, further experiments are done in a dry test rig to analyse a stiffer elastomer. Some parameters' effects under harmonic and static loadings are investigated. Also, the experimental results are validated using finite element-based software, and numerical simulations are in excellent agreement with the Qualisys system's results.

1 INTRODUCTION

The oscillating water column (OWC) device is one of the most promising among available wave energy converters (Heath (2012)). It represents 26.79% of the world's usage of energy converter concepts based on WEC deployment (López et al. (2013); Yacob et al. (2022)). In this device, the air chamber part converts the wave motion to the air pressure, and the power take-off (PTO) system transfers the pneumatic power into electricity (Moretti et al. (2015); Moretti et al. (2020)). Besides several advantages of OWCs, such as high reliability and easy maintenance (Altunkaynak and Çelik (2022)), their simple geometry made them attractive for different researchers to conduct several numerical (Righi et al. (2021)) and experimental analyses (Rezanejad et al. (2017); Moretti et al. (2019); Alizadeh Kharkeshi et al. (2022)). Different types of PTOs have been utilised in the OWCs, such as Bidirectional air turbines (Falcão and Henriques (2016)), Impulse turbines (Henriques et al. (2016)) and dielectric elastomer generators (DEGs) (Vertechy, Papini Rosati, and Fontana (2015)). It is shown that within the range of currently available costs and failure rate, DEGs could reduce the Levelized Cost of Energy (LCOE) by at least a factor of 2 (Teillant et al. (2015)). The advantages of elastomer materials, such as high elongation and fatigue life, have resulted in their wide usage in various types of WECs (Collins et al. (2021)). However, their flexibility and nonlinear behaviour have an inverse effect on the generated power. Different parameters, such as prestretch and

loading frequency, can affect the stiffness of these materials. Finding a relation between stiffness and wave frequency is crucial since the elastomer part's stiffness affects the device's total (hydrodynamic) frequency. Since the upcoming sea wave conditions are measurable and predictable, the OWC position can be adjusted in the most efficient state.

This study conducts several experiments on the water tank and dry test rig to study the effect of different parameters on the elastomer part. The elastomer part is characterised, and a stable hyperelastic model is developed to validate the experimental results with numerical simulation. Several measurement pieces of equipment are utilised to measure the pressure inside the air chamber and water elevation. Also, a very accurate measurement system, the Qualisys optical measurement system, is used to measure the deformation of the elastomer part during tests and the obtained experimental results are validated by numerical simulation.

2 MATERIAL CHARACTERISATION

The material implemented at the top of the OWC corresponds to natural rubber (NR) (Latex grade 'FDA') and a nitrile butadiene rubber (NBR) provided by the companies PAR Group UK and Coruba UK, respectively. The authors have characterised the materials under uniaxial, biaxial, and planar conditions to obtain the wide response of the elastomers under different loads. A computer-controlled Testometric 500X-50 type universal servo-electric test machine with a regularly calibrated 50 kN rated load

cell was employed to measure the properties of the elastomers. At least five samples of each elastomer were evaluated to verify the repeatability of the properties.

Using the mechanical response of the elastomers under uniaxial, biaxial, and planar conditions, the hyperelastic constants of each elastomer were calculated using ABAQUS. A First-order Mooney–Rivlin model (Rivlin (1948)) was a suitable option for both NR and NBR material, showing a stable analytical description. Table 1 summarises both materials' hyperelastic constants according to the chosen model.

Table 1. The First order Mooney–Rivlin model parameters

	Thickness (mm)	C_{10} (MPa)	C_{01} (MPa)
NR			
Blue	0.36	0.5636	0.015
Yellow	0.18	0.5636	0.015
NBR	1.16	0.47	0.16

Also, the first-order Mooney–Rivlin model is represented by the following equation:

$$W = C_{10}(I_1 - 3) + C_{01}(I_2 - 3) \quad (1)$$

where W is the strain energy potential, and I_1 and I_2 are strain invariants (Rivlin (1948)).

3 ABAQUS SIMULATION

In this study, instead of using CFD and fluid-solid interaction analysis, finite element-based software (Abaqus) is used to calculate the deformation of the elastomer and validate the experimental results. In this simulation, pressure transducer data is applied as the loading condition on the surface of the elastomer, and the elastomer is modelled using 4-node bilinear axisymmetric quadrilateral elements (CAX4H). As seen in Figure 1, one side of the elastomer part is fully clamped, and the axisymmetric boundary condition is assumed at the structure's left side (which is the elastomer centre). The nonlinear geometry (NLGEOM) is used to consider the large deformation effect during the analysis.

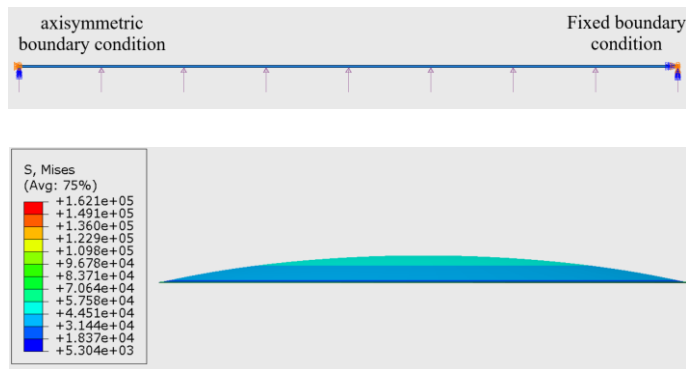


Figure 1. Abaqus simulation and swept view of the result

The following sections present converged results (with four elements in the thickness direction and proper aspect ratio) to validate the experimental results.

4 WATER TANK TEST

This section presents the experimental results of the OWC with the membrane part at the top of the air chamber. The experiments were conducted in the 3D compact wave tank ($9.575 \times 3.150 \times 1.000$ (m)) of the Kelvin Hydrodynamic Laboratory (KHL) of the University of Strathclyde (UK). The tank can produce waves with a period range of 0.5-5 s and a maximum wave height of 0.3 m. Based on the tank characteristics, a small-scale OWC with a scale factor between 1: 30 and 1: 20 was assumed for the prototype based on Froude scaling criteria (Pecher and Kofoed (2017)). Several wave conditions are generated to study the effect of different parameters on the deformation of the membrane part. The OWC model in the water tank and its dimensions are shown in Figure 2. The device consists of an acrylic cylinder and two discs at the top to fix the elastomer material. Also, a fixture is designed and made by a three-dimensional (3D) printing process to fix the device to the supporting structure. The wave probes (made in KHL) consist of two parallel rods; one end is connected to the data acquisition equipment (Micro MKII 1401 made by Cambridge Electronic Design Limited), and the other is below the water surface. Changing the water level between the rods leads to resistance and voltage changes, and after the calibration process, the data from the acquisition system was read by software (Spike2) provided by the same company. Two cameras (Qualisys Oqus 300+) were set above the cylinder, and the deformation was measured using infrared light and specific markers stuck to the membrane. A pressure transducer (Honeywell 163PC01D75) with a range of ± 2.5 in wg was attached near the top of the cylinder to measure the pressure inside the air chamber. In the water tank, waves with different amplitudes and frequencies are generated. Different wave conditions were generated using the wave generator software, and verified by the data from the second wave probe, called the reference wave probe (Ref wp).

The OWC dimensions and the submerged part are designed and chosen to have a natural frequency close to 0.3 Hz. As a result, the deformation of the membrane parts had its highest value at the wave frequency of 0.375 Hz. In this experiment, two natural rubbers (blue and yellow Latex) with different thicknesses are utilised, and their hyperelastic models are presented in Table 1.

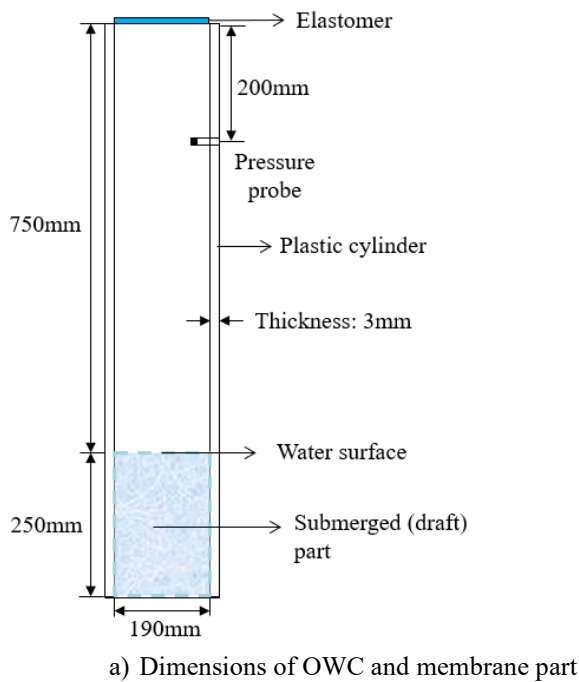


Figure 2. Dimensions of OWC and experimental setup

Figures 3 (a-c) show the results of the Ref wp, wave probe inside the OWC (OWC wp), and pressure transducer of the blue NR related to a specific wave condition (Amplitude=0.01m and Frequency=0.375 Hz). Each experiment took 3 minutes, and in Figure 3, the steady results between 33s and 55s are plotted.

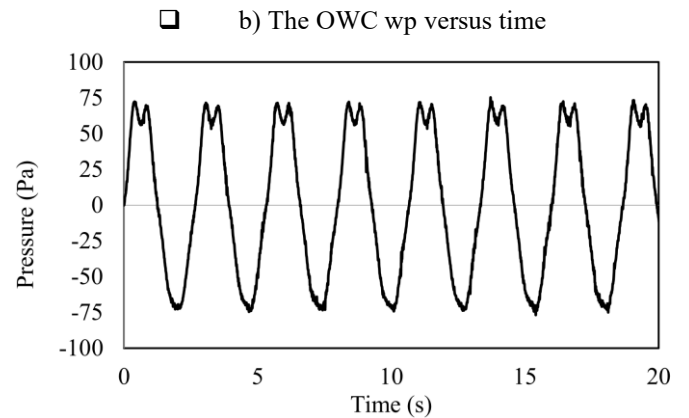
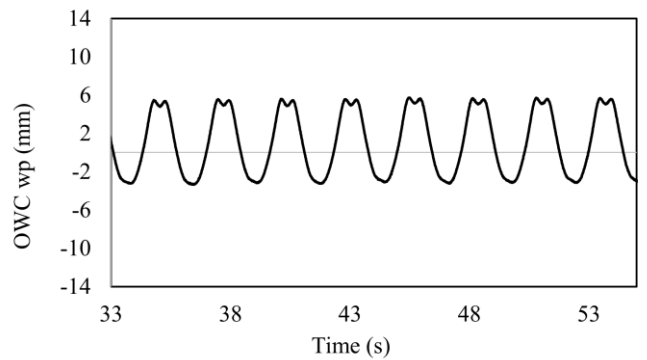
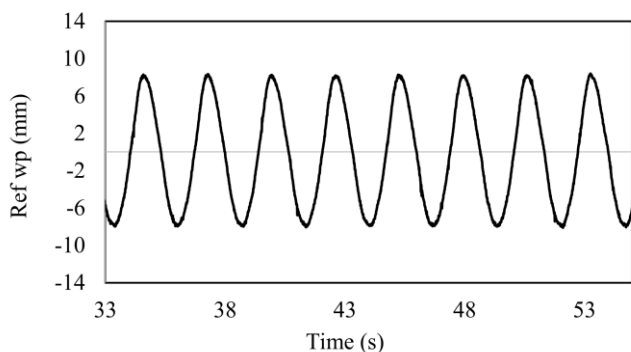


Figure 3. Pressure and wave elevation results in a wave with an amplitude of 0.01 m and Frequency of 0.375 Hz.

Figure 4 shows the deformation at the elastomer's centre (tip displacement) measured by the Qualisys system and Abaqus simulation. It can be seen that the amplitude of deformation in the experiment is less than Abaqus. While fixing the elastomer at the top of the air chamber, we may have applied an unwanted prestretch on the elastomer, leading to higher stiffness and lower deformation than the numerical simulation.

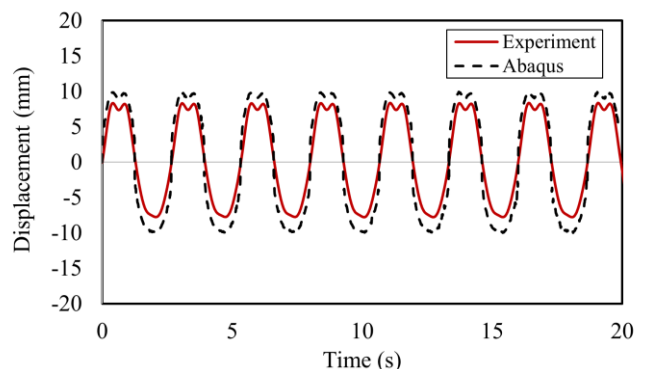


Figure 4. Experimental and numerical results of tip displacement versus time (Wave amplitude=0.01m and Frequency=0.375 Hz)

In the next step, different waves with various wave frequencies (and constant amplitude) are generated to study the wave frequency's effect on elastomer stiffness. Figure 5 shows the pressure versus tip displacement results in a half-cycle for the highest and

lowest frequencies. The trendline of each curve is plotted, and different gradients prove that the stiffness of the elastomer part depends on the wave frequency.

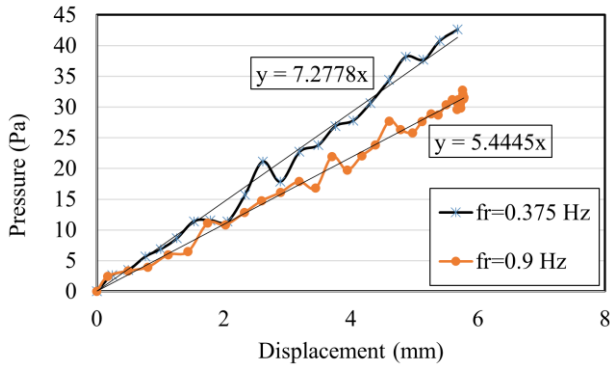


Figure 5. Pressure versus displacement with different loading frequencies

Also, Figure 6 shows the pressure versus tip displacement results in a static test, and its slope is almost equal to that of the lowest frequency in Figure 5. For the static test, we pushed the cylinder down to the water (4 mm for each step) and captured the deformation and pressure inside the air chamber. As seen in figure 6, the linear approximation line has a constant value of 21.146. However, it should be mentioned that in zero pressure, the deformation leads to zero due to the nonlinear stiffness of the elastomer.

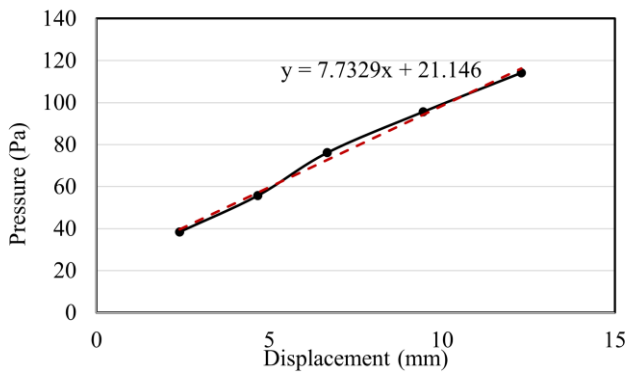


Figure 6. Pressure versus tip displacement in the static test

Furthermore, the response amplitude operator (RAO) versus wave amplitudes is plotted in Figure 7 for both blue and yellow Latex. It can be seen that the yellow Latex, which has lower thickness and stiffness, has a higher RAO value compared with the blue one.

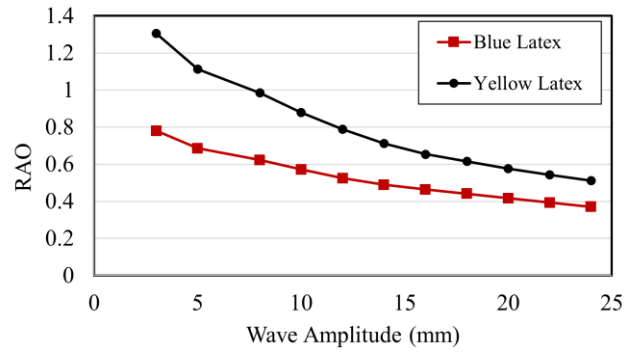


Figure 7. Effect of the response amplitude operator (RAO) for different wave amplitudes

5 DRY TEST RIG:

In the previous section, some water tank results were presented. However, due to the pressure limitation inside the air chamber and to have enough deformation, we could use Latex as the elastomer part. A laboratory's dry test rig is designed and built (Fig. 8) to overcome this limitation and do more experiments with stiffer and thicker material. A brushless linear servo motor (model 50206012F-LCE-CV provided by MOOG company) is used to apply the harmonic loading on the piston part. In the designed test rig, the amount of actuator stroke changes the pressure in the air chamber and deforms the elastomer part. The same pressure transducer and Qualisys system are used to measure the pressure inside the air chamber and the deformation of the elastomer part.

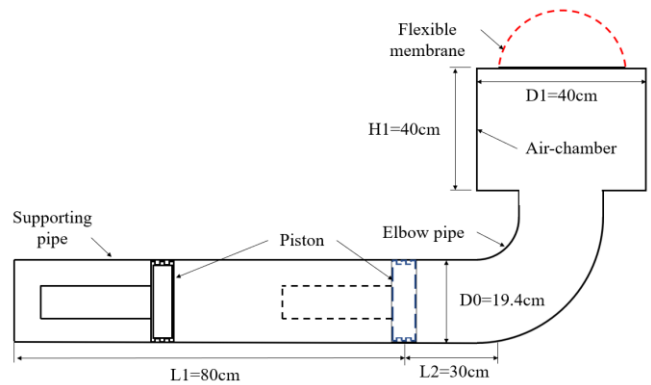
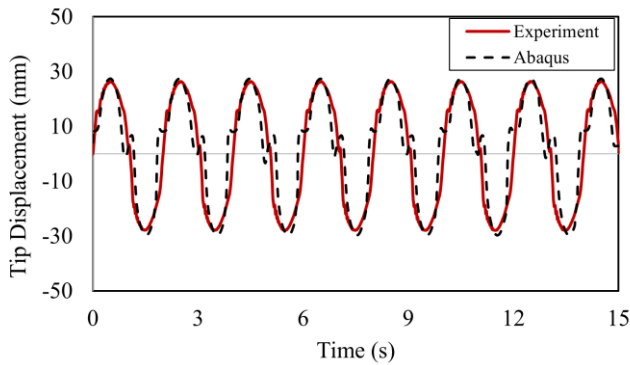


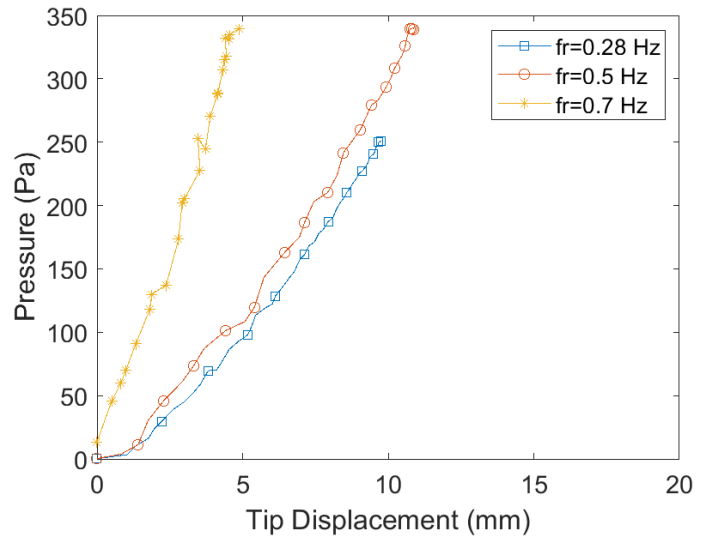
Figure 8. The schematic diagram of the designed dry test rig

In this section, a Nitrile Butadiene Rubber (NBR) with a thickness of 1.16 mm is attached at the top of the air chamber, and its material properties are characterised and shown in Table 1. For this section, two series of experiments are conducted. For this section, two series of experiments are conducted. The material is put at the top of the air chamber without prestretch in the first part. Due to the specimen's scale and weight, the elastomer without prestretch has a non-zero deformation at zero pressure. This issue affects the pressure inside the air chamber, and as shown in Figure 9, results have a slight oscillation close to the zero-deformation line. Since the sensitivity of the pressure transducer is more than the Qualisys system, the fluctuation is more noticeable in Abaqus results. This problem interrupts DEG's energy production and makes us apply prestretch to the elastomer part. The Qualisys system data for a stroke frequency of 0.5 Hz is validated by the Abaqus simulation (Figure 9).



□ Figure 9. Experimental and numerical results of tip displacement versus time

Figure 10 shows the pressure versus tip displacement for different loading frequencies. To plot this figure, various tests with the same actuator stroke and different frequencies are conducted. As seen in Figure 10, increasing the frequency rate leads to an increase in the stiffness of the elastomer part, which proves that the total frequency of the OWC can be affected by various wave periods.

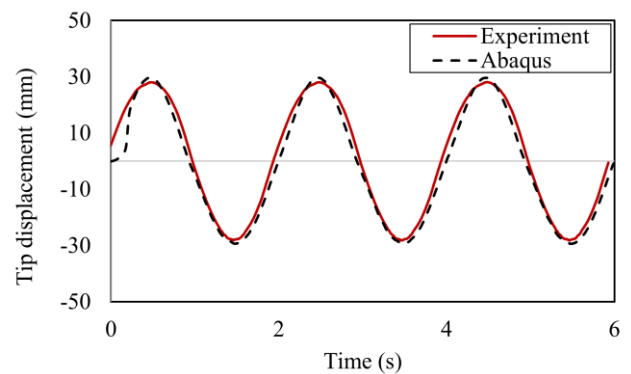


□ Figure 10. The pressure versus tip displacement for different loading frequencies

In the second part, the material is pre-stretched according to the following relation:

$$\lambda = e/e_0 \quad (2)$$

In which e and e_0 are the frame and undeformed membrane radii, respectively. Since applying the prestretch increases the elastomer stiffness and reduces the deformation (in this deformation mode), a small amount of prestretch ($\lambda=1.05$) is considered. Figure 11 shows the tip displacement versus time and its validation with the Abaqus simulation. The numerical simulation has the same elements and modelling approach as the previous simulations, except for adding a primary step to apply prestretch.



□ Figure 11. Experimental and numerical results of tip displacement versus time

Also, Figure 12 illustrates pressure versus tip displacement for different stroke frequencies. Due to applying prestretch, the difference between the stiffness of different cases is slight. However, the difference between curves grows after the tip displacement of 15 mm, which makes us apply a higher stroke and deformation. Since the current linear actuator has a limitation of 25 cm stroke, we will continue this study with a new linear actuator and more deformation in the future.

7 CONCLUSIONS

This study conducts several experiments on the water tank and dry test rig to study the effect of different parameters on elastomer stiffness. The elastomer part is characterised by uniaxial, biaxial, and planar tests and the obtained First-order Mooney–Rivlin model is used in the numerical simulation to validate the water tank and test rig results. Different tests are conducted to prove the dependency of the elastomer stiffness on the loading frequency. It is shown that increasing the loading frequency leads to an increase in the elastomer's stiffness.

Furthermore, the effect of pre-stretching on the deformation and stiffness of the elastomer is studied. It is proved that in this deformation mode, the pre-stretch can increase and decrease the stiffness and deformation of the elastomer, respectively.

8 REFERENCES

- Alizadeh Kharkeshi, Behrad, Rouzbeh Shafaghat, Omid Jahanian, Rezvan Alamian, and Kourosh Rezanejad. 2022. Experimental study on the performance of an oscillating water column by considering the interaction effects of optimal installation depth and dimensionless hydrodynamic coefficients for the Caspian Sea waves characteristics, *Ocean Engineering*, 256: 111513.
- Altunkaynak, Abdüsselam, and Anıl Çelik. 2022. A novel Geno-fuzzy based model for hydrodynamic efficiency prediction of a land-fixed oscillating water column for various front wall openings, power take-off dampings and incident wave steepnesses, *Renewable Energy*, 196: 99-110.
- Collins, Ieuan, Mokarram Hossain, Wulf Dettmer, and Ian Masters. 2021. Flexible membrane structures for wave energy harvesting: A review of the developments, materials and computational modelling approaches, *Renewable and Sustainable Energy Reviews*, 151: 111478.
- Falcão, A. F. O., and J. C. C. Henriques. 2016. Oscillating-water-column wave energy converters and air turbines: A review, *Renewable Energy*, 85: 1391-424.
- Heath, TV. 2012. A review of oscillating water columns, *Philosophical Transactions of the Royal Society A: Mathematical, Physical and Engineering Sciences*, 370: 235-45.
- Henriques, J. C. C., J. C. C. Portillo, L. M. C. Gato, R. P. F. Gomes, D. N. Ferreira, and A. F. O. Falcão. 2016. Design of oscillating-water-column wave energy converters with an application to self-powered sensor buoys, *Energy*, 112: 852-67.
- López, Iraide, Jon Andreu, Salvador Ceballos, Iñigo Martínez de Alegría, and Iñigo Kortabarria. 2013. Review of wave energy technologies and the necessary power-equipment,

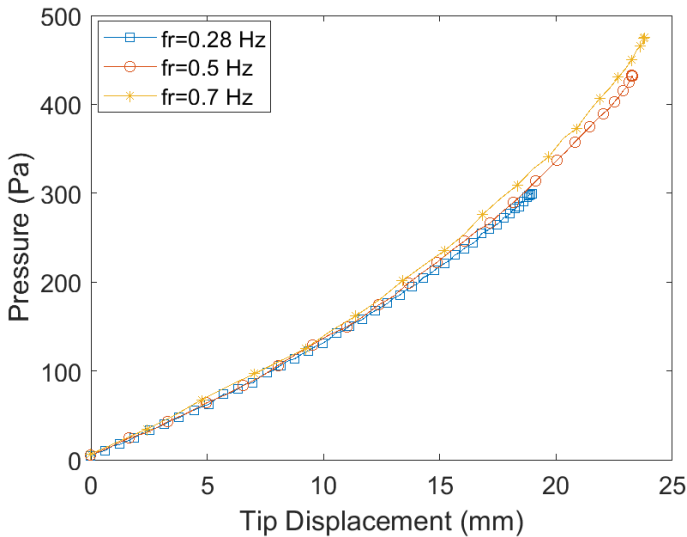


Figure 12. The pressure versus tip displacement for different loading frequencies

Figure 13 depicts the experimental results of the tip displacement of elastomer with and without pre-stretch for the stroke frequency of 0.28 Hz. This figure aims to show the effect of pre-stretching on the stiffness of the elastomer part. It can be seen from the figure that pre-stretching leads to an increase in the material stiffness in this mode of deformation. It should be mentioned that the prestretch of materials may affect their stiffness differently based on the deformation mode.

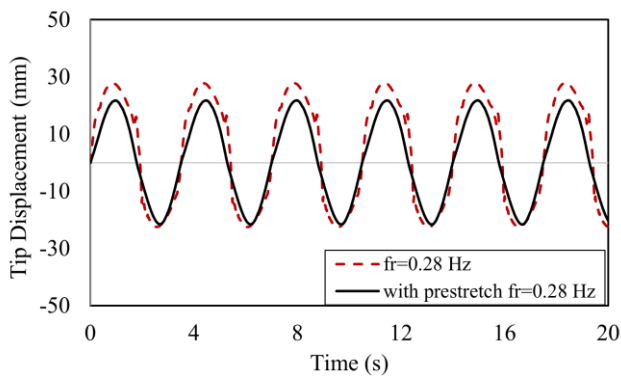


Figure 13. The tip displacement of elastomer with and without prestretch versus time

6 ACKNOWLEDGMENTS

This work was supported by the Centre for Bionic Adaptive Stretchable Materials for Wave Energy Converters (BASM-WEC) under grant number EP/V040553/1 from the UK Engineering and Physical Sciences Research Council (EPSRC).

Renewable and Sustainable Energy Reviews, 27: 413-34.

- Moretti, G., G. Malara, A. Scialò, L. Daniele, A. Romolo, R. Vertechy, M. Fontana, and F. Arena. 2020. Modelling and field testing of a breakwater-integrated U-OWC wave energy converter with dielectric elastomer generator, *Renewable Energy*, 146: 628-42.
- Moretti, G., G. P. R. Papini, L. Daniele, D. Forehand, D. Ingram, R. Vertechy, and M. Fontana. 2019. Modelling and testing of a wave energy converter based on dielectric elastomer generators, *Proceedings of the Royal Society A: Mathematical, Physical and Engineering Sciences*, 475.
- Moretti, Giacomo, Gastone Pietro Papini Rosati, Marco Alves, Manuel Grases, Rocco Vertechy, and Marco Fontana. 2015. "Analysis and design of an oscillating water column wave energy converter with dielectric elastomer power take-off." In *International Conference on Offshore Mechanics and Arctic Engineering*, V009T09A23. American Society of Mechanical Engineers.
- Pecher, Arthur, and Jens Peter Kofoed. 2017. *Handbook of ocean wave energy* (Springer Nature).
- Rezanejad, K., C. Guedes Soares, I. López, and R. Carballo. 2017. Experimental and numerical investigation of the hydrodynamic performance of an oscillating water column wave energy converter, *Renewable Energy*, 106: 1-16.
- Righi, Michele, Giacomo Moretti, David Forehand, Lorenzo Agostini, Rocco Vertechy, and Marco Fontana. 2021. A broadbanded pressure differential wave energy converter based on dielectric elastomer generators, *Nonlinear Dynamics*, 105: 2861-76.
- Rivlin, Ronald S. 1948. Large elastic deformations of isotropic materials IV. Further developments of the general theory, *Philosophical transactions of the royal society of London. Series A, Mathematical and physical sciences*, 241: 379-97.
- Teillant, Boris, Giacomo Moretti, Rocco Vertechy, Marco Fontana, Kieran Monk, and Marco-Filipe Alves. 2015. "Techno-economic comparison between air turbines and dielectric elastomer generators as power take off for oscillating water column wave energy converters." In.
- Vertechy, R., G. P. Papini Rosati, and M. Fontana. 2015. Reduced model and application of inflating circular diaphragm dielectric elastomer generators for wave energy harvesting, *Journal of Vibration and Acoustics, Transactions of the ASME*, 137.
- Yacob, D. H., S. Sarip, H. M. Kaidi, J. A. Ardila-Rey, and F. Muhammad-Sukki. 2022. Oscillating Water Column Geometrical Factors and System Performance: A Review, *IEEE Access*, 10: 32104-22.